Examination of the Tsunami Generated by the 1906 San Francisco M_w=7.8 Earthquake, Using New Interpretations of the Offshore San Andreas Fault

By Eric L. Geist and Mary Lou Zoback

CONTENTS

Abstract

From new interpretations of the geometry of the San Andreas Fault geometry offshore of the Golden Gate, we demonstrate that the tsunami from the great 1906 San Francisco M_w=7.8 earthquake is best explained by bilateral rupture on discontinuous fault segments starting at an epicentral location near an offshore dilatational stepover north of Lake Merced. To establish this inference, we use elastic dislocation and hydrodynamic models to analyze the tsunami. We compare various scenarios involving different rupture geometries and physical properties with the record of the tsunami at the Presidio tide-gauge station in the northwestern part of San Francisco. A tsunami generated from a continuous rupture on the San Andreas Fault west of the Golden Gate is insufficiently small and has an arrival time earlier than what was observed, whereas a tsunami generated from discontinuous rupture defined by the 3-km dilatational stepover north of Lake Merced and a 1-km compressional stepover south of Bolinas Lagoon better explains the observed arrival time and waveform. It is unclear from our analysis, however, whether the observed peak negative amplitude is better explained by a local change in rake at the dilatational stepover (consistent with analysis of the genetically similar 1995 Kobe, Japan, M_w=6.9 earthquake) or by large-scale exceedance of the strength of rocks surrounding the fault (modeled by a material that conserves volume during deformation). The apparent epicentral locations for both the 1906 San Francisco and 1995 Kobe, Japan, earthquakes at dilatational stepovers suggest that the initial stress in these regions is conducive to earthquake initiation. With respect to the hydrodynamics of the tsunami, the modeled evolution of the tsunami wavefield propagating from the source region indicates that the oscillations with a dominant period of 40 to 45 minutes observed in the coda of the tsunami record are best explained by the natural resonance of trapped edge waves in the Gulf of the Farallones, rather than by reverberation of the tsunami within San Francisco Bay.

Introduction

The 1906 San Francisco M_w=7.8 earthquake is commonly considered a baseline event for defining earthquake hazards in the San Francisco Bay region (fig. 1). Such hazard parameters as peak ground acceleration, accumulated slip, and segmentation all depend on accurate analysis of this event. Although many studies have examined this event, definition of the detailed rupture process is hampered by an absence of near-field instrumental records. Bolt (1968) and Boore (1977) used the only near-field recording of the earthquake in combination with teleseismic records to constrain the epicentral location of the 1906 earthquake. Wald and others (1993) used recordings of the 1984 Morgan Hill, Calif., M_w=6.2 earthquake to derive empirical Green's functions for the 1906 earthquake; they were able to resolve an asperity less than 40 km long in the area between Point Reyes and Fort Ross from teleseismic recordings of the 1906 earthquake. Recently, Thatcher and others (1997) reexamined data from regional and local geodetic networks to infer the slip distribution in places along the fault.

Another type of near-field recording that can aid in the determination of rupture parameters is the tide-gauge record of a tsunami resulting from the 1906 San Francisco earthquake. The 1906 earthquake rupture propagated bilaterally along the offshore section of the San Andreas Fault seaward of the Golden Gate (fig. 1). The only tide gauge in northern California operating at that time was located in San Francisco, only 10 km from the offshore trace of the San Andreas Fault. In this study, we use this tide-gauge record to constrain the offshore rupture geometry of the 1906 earthquake. The essentials of this study were first presented by Geist and

Zoback (1999); we present here more detailed information on the modeling technique used, the various source mechanisms examined, and the evolution of the tsunami wavefield in San Francisco Bay and the Gulf of the Farallones.

Because of the small size of the tsunami recorded from the 1906 earthquake, the actual local tsunami hazard in the San Francisco Bay region is low in comparison with the ground-shaking hazard from a similar event. The main contribution of this study is to provide supporting evidence for a 3-km right stepover in the offshore San Andreas Fault, recently discovered by detailed analysis of high-resolution aeromagnetic data (Jachens and Zoback, 1999; Zoback and others, 1999). The effect of a dilatational stepover on rupture dynamics, however, is unclear. Segall and Pollard (1980) showed that the normal stress on the fault decreases for a dilatational step, facilitating sliding, but may also provide a relaxation barrier to rupture, as described by Das and Aki (1977). Evidence from the 1995 Kobe, Japan, earthquake (Wald, 1996) and the 1906 San Francisco earthquake (Zoback and others, 1999) also suggests that earthquakes may preferentially initiate at dilatational steps. An accurate definition of the rupture geometry near the epicenter of the 1906 earthquake is needed to better understand the rupture dynamics of the San Andreas Fault in the San Francisco Bay region.

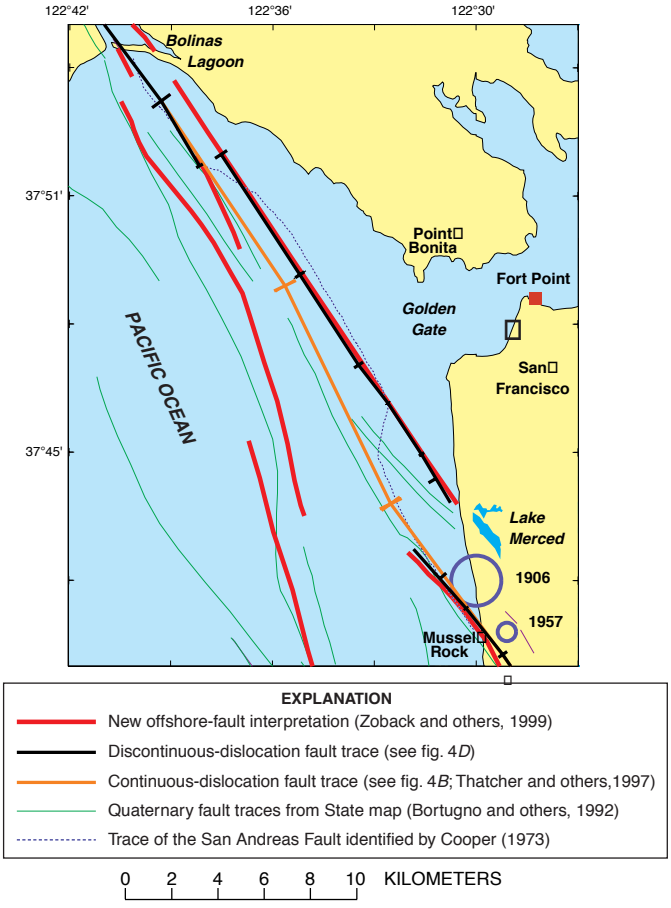

Figure 1.—San Francisco Bay region, showing possible fault geometries on the Golden Gate platform. Inferred offshore fault structure is determined from gradient analysis of new high-resolution aeromagnetic data (Jachens and Zoback, 1999; Zoback and others, 1999). Hachures, boundaries of individual fault segments used in dislocation modeling; circles, epicenters of 1906 M_w=7.8 (Bolt, 1968) and 1957 M=5.3 probable normal-faulting earthquakes (Marsden and others, 1995).

Background

The 1906 San Francisco earthquake, which occurred at 5:12 a.m. P.s.t. on April 18, 1906, was recorded by 96 seismic stations around the world but by only one local seismic station, located at the Lick Observatory on Mount Hamilton (Lawson, 1908). In the months after the earthquake, a comprehensive report was published by Andrew Cowper Lawson describing not only seismic observations but also geologic effects and various circumstantial measurements, including the tidal anomaly recorded at the Presidio tide-gauge station. A review of tidal observations for the 9 years preceding the earthquake showed that for at least the period 1903–6, no change occurred in the sea-level datum at the Presidio. Without the aid of the numerical hydrodynamic models at our disposal today, Lawson was able only to conjecture as to the origin of the recorded tsunami. On the basis of its traveltime, Lawson suggested that the tsunami arose from sea-floor subsidence west of the fault trace, interpolated to the offshore region. Although this suggestion seemed to contradict onland observations of permanent ground movement associated with the earthquake, it was supported at the time by Harry Fielding Reid (who later would develop the theory of elastic rebound; see Reid, 1910) in a note to Lawson:

If a depression occurred on the western side of the faultline, extending for some distance to the westward, it would start a wave of depression towards the Golden Gate which would take 9 minutes to reach Fort Point, and this is just about the time recorded by the gage. The time necessary for the recovery to normal level would depend upon the extent of the area depressed. If this were a narrow block, a wave of elevation would follow quickly upon the wave of depression, and we should have a rapid elevation of the tide-gage above its normal position. As no such wave appeared and recovery was very gradual, we must suppose that the deprest area extends for some distance to the westward, so that the recovery was slow. This is the only explanation so far offered that would produce the effects observed.

Today, we have much better insight as to the tectonic setting of the San Francisco Bay region, as well as to the dynamics of the 1906 earthquake. As we show in this chapter, however, we are still struggling to explain, as was Reid, the unusual tsunami record at the Presidio tide-gauge station.

Previous analysis of this tsunami by Ma and others (1991) focused on determining the pattern of sea-floor deformation from a linear inversion of the tide-gauge record. The resolved pattern of uplift and subsidence is complex but largely reflects subsidence west of the fault, as originally suggested by Lawson (1908). Ma and others (1991) concluded that the subsidence resulted from the overall dilatational fault

geometry and that a large component of dip slip for the earthquake was not needed to explain the tsunami record.

Since the study by Ma and others (1991), Zoback and others (1999) reinterpreted the seismotectonics of the San Andreas Fault in the San Francisco Bay region. They used high-resolution aeromagnetic and multichannel seismic-reflection data, in combination with relocated seismicity and focal-mechanism determinations, to detail the offshore fault geometry of the Golden Gate platform (fig. 1). The newly defined offshore trace of the San Andreas Fault includes a 3-km right (dilatational) step directly northwest of Lake Merced and a smaller, 1-km left (compressional) step near Bolinas Lagoon (fig. 1). Interestingly, the interpreted fault traces are closely aligned with the "recent trace" of the San Andreas Fault identified by Cooper (1973), using older, single-channel seismic-reflection data. Also, the location of the dilatational step northwest of Lake Merced approximately coincides with the epicenter of the 1906 earthquake as determined by Bolt (1968).

In this chapter, we use the offshore fault geometry as newly defined by Zoback and others (1999) and the slip of the event as estimated by Thatcher and others (1997) to construct a forward model for the tsunami. We examine different rupture scenarios in which the stepover geometry and rake of the slip vector vary, and we compare the results with the Presidio tide-gauge record. We also investigate whether sources other than rupture on the San Andreas Fault, such as a triggered normal-fault earthquake or a coseismically triggered failure of nearby coastal cliffs, could explain the observed tsunami.

In addition to constraining the rupture process of the 1906 earthquake, this tsunami model also helps us better understand the wave dynamics in the offshore region and in San Francisco Bay from a locally generated tsunami. Several sea-level oscillations following the initial wave with an apparent period of 40 to 45 minutes were observed on the Presidio tide-gauge record. Lawson (1908) ascribed this phenomenon to reverberation of the tsunami in San Francisco Bay, between Berkeley and Fort Point (fig. 1). With a calibrated tsunami model, we can better understand the origin of these oscillations and the overall evolution of the tsunami.

Interpretation of the Offshore San Andreas Fault

In the southern part of the San Francisco peninsula, the San Andreas Fault makes a broad (~10º–11º) left (restraining) bend and is situated in a valley following the crest of the late Pliocene through Quaternary Coast Ranges (for example, Bürgmann and others, 1994). Less than 70 km to the northwest, the San Andreas Fault trace is below sea level. Projection of the onshore traces northwest of Lake Merced and southeast of Bolinas Lagoon suggests a 2- to 3-km right step or bend offshore on the Golden Gate platform (fig. 1). Linear pseudogravity maximum gradients inferred from the shortest wavelengths in a new high-resolution aeromagnetic survey reveal in detail a right-stepping geometry for both the San Andreas and subparallel San Gregorio Fault zones on the Golden Gate platform (Jachens and Zoback, 1999; Zoback and others, 1999).

In this study, we have incorporated an ~3-km right step in the San Andreas Fault just offshore from Lake Merced (fig. 1), following Jachens and Zoback (1999) and Zoback and others (1999). The position of this inferred right step (fig. 1) is consistent with the interpretation of the "recent trace" of the San Andreas Fault from single-channel high-resolution seismic-reflection profiles by Cooper (1973). The newly defined easternmost strand of the San Andreas Fault extends northwestward to the east side of Bolinas Lagoon (fig. 1), whereas the 1906 earthquake rupture lies along the west side of Bolinas Lagoon, implying an additional small (~1 km) left step offshore. Cooper also identified such a left step in his interpretation of the San Andreas Fault just north of lat 37º51′ N. (fig. 1), where the San Andreas Fault trace mapped by him coincides with the fault segment inferred from aeromagnetic analysis that connects with the surface trace of the 1906 earthquake rupture on the west side of Bolinas Lagoon. Thus, the available offshore data suggest an ~3-km extensional right step and a smaller (~1 km) compressional left step in the San Andreas Fault on the Golden Gate platform (fig. 1). Bolt's (1968) teleseismic location for the 1906 earthquake is close to the right stepover (fig. 1). Zoback and others (1999) have suggested that the bilateral 1906 earthquake rupture may have initiated in the right stepover region of the San Andreas Fault, on the basis of similarities to the bilateral 1995 Kobe, Japan, earthquake rupture, which also initiated at a similar right step in a right-lateral fault (Wald, 1996). Segall and Pollard (1980) demonstrated that normal traction along a right-lateral fault decreases at a right-stepping discontinuity, facilitating sliding.

Tsunami Record

The tsunami from the 1906 San Francisco earthquake was recorded at the U.S. Coast and Geodetic Survey's Presidio tide-gauge station, which has been in operation since July 15, 1897. In the early 1900s, the station was located at the Presidio Wharf at the east end of the Presidio Military Reservation, approximately 1.5 km east of the tide-gauge station currently operated by the National Oceanic and Atmospheric Administration near Fort Point (fig. 1; Disney and Overshiner, 1925). A detailed description of the standard automatically recording tide gauge was given by Bowditch (1966).

The first arrival of the tsunami from the 1906 earthquake was recorded as a 10-cm lowering of sea level for a period of ~16 minutes (fig. 2*A*). Lowering of sea level commenced approximately 7.5 minutes after the earthquake, although absolute timing is uncertain, as described below. Unlike on most tide-gauge recordings of tsunamis (fig. 2*B*), no positive deflection of sea level followed the initial solitary depression. A series of two to three oscillations with an apparent period of 40 to 45 minutes and a maximum amplitude of 5 cm were recorded approximately a half-hour after the initial solitary depression (fig. 2*A*). Likewise, distant tsunamis recorded at

this tide-gauge station are characterized by a solitary wave (commonly bipolar, however) followed by an oscillatory coda, as exemplified by the recording of the tsunami from the 1960 Chile M_w=9.6 earthquake (fig. 2*B*; Lander and others, 1993). During the time of the 1906 earthquake, ambient short-period wave energy due to meteorologic effects is apparent in the tide-gauge record for 2 days before the earthquake, slowly diminishing but continuing while the tsunami was recorded (fig. 2*A*; Disney and Overshiner, 1925).

The tide-gauge record was digitized at a sampling rate of 7 s, corrected to remove the tidal signal, and then analyzed. The tidal signal was removed from the digitized tide-gauge record by calculating tidal harmonic constants for the observation site (Foreman, 1993). Absolute timing of the tide-gauge record is uncertain for the following reasons. (1) In comparison with the astronomical clocks stopped by the earthquake, the running clock of the tide gauge was probably too slow, whereby the earthquake was indicated by blurring of the tide-gauge pencil mark (Lawson, 1908). (2) The timing marks on the record are generally ambiguous as to where they cross the sea-level curve. The time interval between the blurring mark and the initial lowering of sea level appears to be 7.5 minutes, although Lawson indicated that the time interval was 9 to 10 minutes. (The direct *P*-wave traveltime would be ~3 s, with a direct *S*-wave arriving ~2 s later, assuming average *P*- and *S*- wave velocities of 5.7 and 3.3 km/s, respectively; Holbrook and others, 1996.)

We calculated the power spectrum of the tide-gauge record at three different 2-hour time windows to determine the dominant periods of the tsunami (fig. 3). Rabinovich (1997) explained that the nearshore wave spectrum of a tsunami can be separated into components dependent on the source parameters of the earthquake and the natural resonant periods of the nearshore bathymetry. The first time window, 3:00–5:00 a.m. P.s.t., shows the spectrum for the 2 hours before the tsunami. The short-period-wave energy is mainly within two frequency ranges: 11–13 cycles per hour and 20–24 cycles per hour. Disney and Overshiner (1925) attributed this wave energy to a wind-generated imperfect oscillation across the Golden Gate (fig. 1). In the second time window, 5:00–7:00 a.m., the tsunami energy is apparent in the frequency range 2–4 cycles per hour and is largely dictated by the source parameters of the earthquake. Interestingly, wave energy at 11 to 13 cycles per hour is subdued during the 2 hours after the earthquake. The wind-generated oscillation across the Golden Gate may have been interrupted by the passage of the tsunami and then gradually resumed (presumably, the wind forcing continued over this time). Conceivably, the seismic compressive waves propagating through the water column may have disrupted the self-organization of the surface waves, in much the same way (though on a smaller scale) that vortex rings produced by raindrops disrupt surface waves (Poon and others, 1992; Tsimplis, 1992). We cannot exclude the possibility, however, that the response of the tide gauge was somehow temporarily affected by the ground shaking. In the third time window, 7:00–9:00 a.m., the wave energy at 11 to 13 cycles per hour is again apparent, as is lower-frequency energy from oscillations excited by the tsunami, owing to resonant periods of the bathymetry within the Gulf of the Farallones (see Eva and Rabinovich, 1997).

Tide gauges are designed to record energy that occurs at tidal periods (diurnal and semidiurnal) and to attenuate shorter-period wave energy. Tsunamis typically occupy a gap in the wave spectrum between tidal periods and the short periods of wind-generated waves. Although tsunami periods are shorter than tidal periods, they are not as greatly attenuated as wind-generated waves. Several workers have examined the response of tide gauges to tsunamis (Cross, 1968; Loomis, 1983; Satake and others, 1988). The response of most tide gauges installed by the U.S. Coast and Geodetic Survey is distinctly different from that of the tide gauges used in Japan (Satake and others, 1988). For U.S. tide gauges, the outflow is faster than the inflow, whereas for Japanese gauges, the opposite is the case. The response of tide gauges is nonlinear and frequency dependent. For tsunami waves of small amplitude (<1.5 m) and long period (>12 minutes), such as the tsunami from the 1906 San Francisco earthquake, there is little attenuation in amplitude and little lag in the response of the tide gauge relative to the actual wave (Cross, 1968; Loomis, 1983).

Hydrodynamic Modeling

During an earthquake, coseismic vertical displacement of the sea floor creates a gravitational instability in the water column that generates a tsunami. Because of the large wavelength of the coseismic displacement field, the length of the initial tsunami wave is nearly identical to the displacement at the sea floor. Only when the wavelength of displacement is less than about 3 times the water depth, or in regions of very steep bathymetry, do special modifications need to be made in approximating the initial tsunami wavefield to the vertical coseismic displacement. During propagation, the gravitational potential energy is transferred to kinetic energy, such that the wave travels at a long-wave phase velocity c, of $c = \sqrt{gh}$, where g is the gravitational acceleration (in meters per second squared) and h is the water depth (in meters). The large wavelength of tsunamis also permits us to use the following shallow-water-wave equations to describe the evolution of the tsunami during propagation and, eventually, to reconstitute the wave recorded at the tide gauge station:

$$\frac{\partial(\eta + h)}{\partial} + \nabla \cdot [v(\eta + h)] = 0 \qquad \text{(continuity equation)}$$

and

$$\frac{Dv}{Dt} + g\nabla\eta + \gamma v = 0 \qquad \text{(momentum equation)}$$

where η is the water-surface elevation, v is the depth-averaged horizontal-velocity field, and γ is the bottom-friction coefficient. The substantial derivative is given by

$$\frac{Dv}{Dt} = \frac{\partial}{\partial t} + (v \cdot \nabla).$$

To model the tsunami from the 1906 San Francisco earthquake, we modify the TRIM (tidal, residual, intertidal mudflat) shallow-water-circulation model of Casulli (1990) and Cheng and others (1993) that has been extensively used to study tidal and residual circulation in San Francisco Bay. Several recent examples have shown how sophisticated estuarine-circulation models can be used for regional tsunami studies (Peraire and others, 1986; Greenberg and others, 1993; Myers and Baptista, 1995; Tinti and Piatanesi, 1996).

The TRIM model is based on a semi-implicit, finite-difference numerical approximation of the nonlinear shallow-water-wave equations. Hydrostatic pressure is assumed, and so dispersive effects, which are commonly observed for far-traveled tsunamis, are unaccounted for. Unlike many fully explicit finite-difference techniques used to model tsunami propagation, the TRIM model uses a semi-implicit technique to achieve unconditional stability, and so does not need to satisfy the Courant-Friederichs-Lewy (CFL) stability condition. The TRIM model also avoids spurious numerical effects at channel constrictions that are present with alternating-direction implicit (ADI) methods. The velocity-divergence term in the continuity equation and the water-surface-gradient term in the momentum equations are finite-differenced explicitly, whereas the remaining terms are finite-differenced implicitly (Casulli, 1990; Cheng and others, 1993). In addition, a Eulerian-Lagrangian method is used to calculate

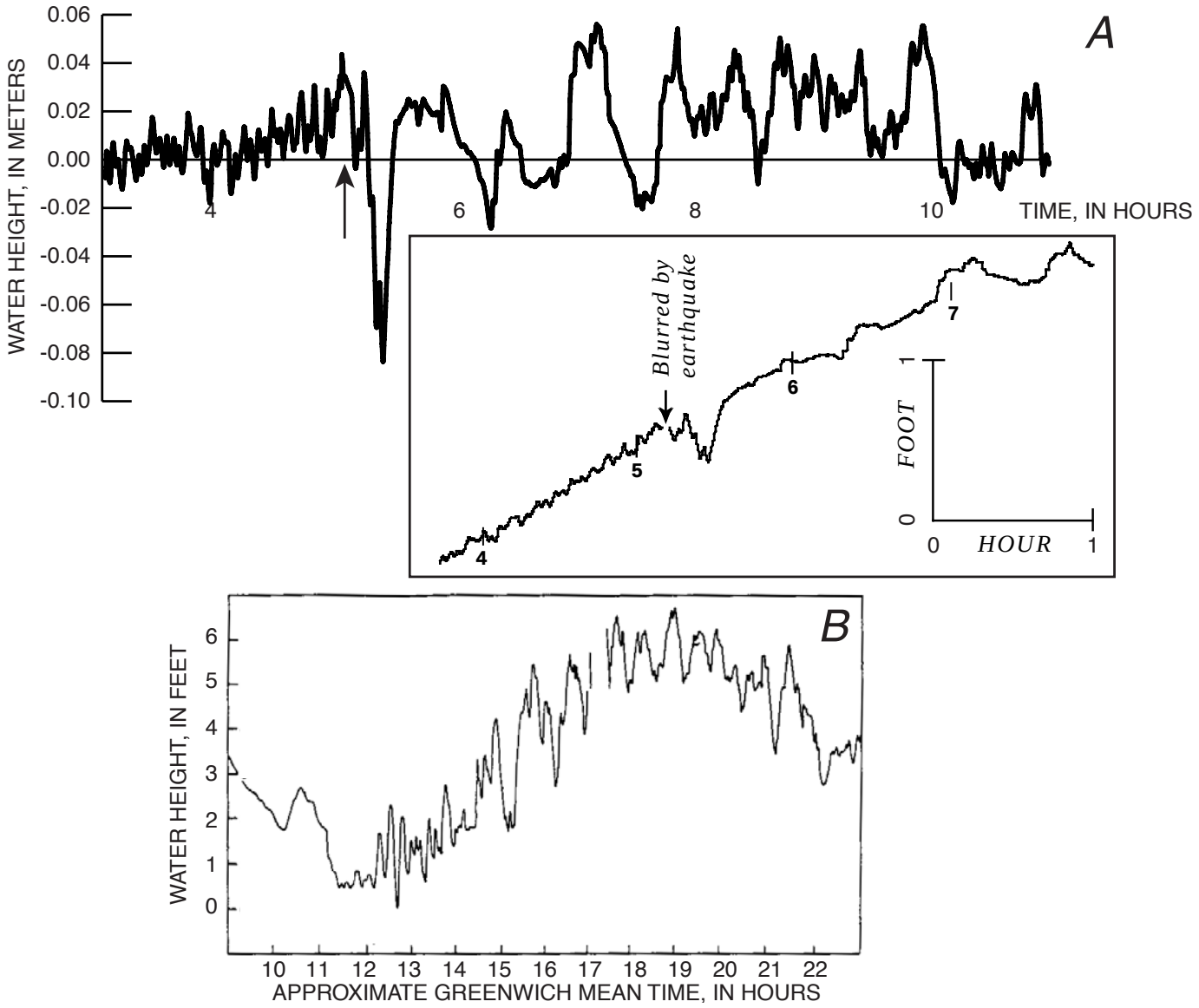

Figure 2.—Tsunami records. *A*, Tsunami from 1906 San Francisco earthquake recorded at the Presidio tide-gauge station, with tidal signal removed. Arrow denotes approximate origin time of earthquake. Inset shows original, uncorrected record from Lawson (1908). *B*, Tsunami from April 22, 1960, M_w=9.6 earthquake recorded at the Presidio tide-gauge station (uncorrected). Note difference in waveform of source signal (first arrival), followed by natural resonance excited by tsunami.

the convective terms. The bilinear interpolation used in the Eulerian-Lagrangian method gives rise to artificial diffusion, which may be a concern for tsunami-propagation applications (P.L.-F. Liu, oral commun., 1998). Cheng and others demonstrated that the artificial diffusion is functionally dependent on the grid size and that for the fine-grid scales used in many regional estuary studies (~250 m), this artifact is not a significant problem.

To use the TRIM model for tsunami propagation, boundary and initial conditions need to be modified. Because the data for comparison is the residual tide-gauge record with the tidal component removed, tidal forcing along the open boundaries of the model is replaced with passive, radiation boundary conditions (Reid and Bodine, 1968). Assuming incompressibility in the water column, initial conditions are specified by the vertical coseismic displacement field

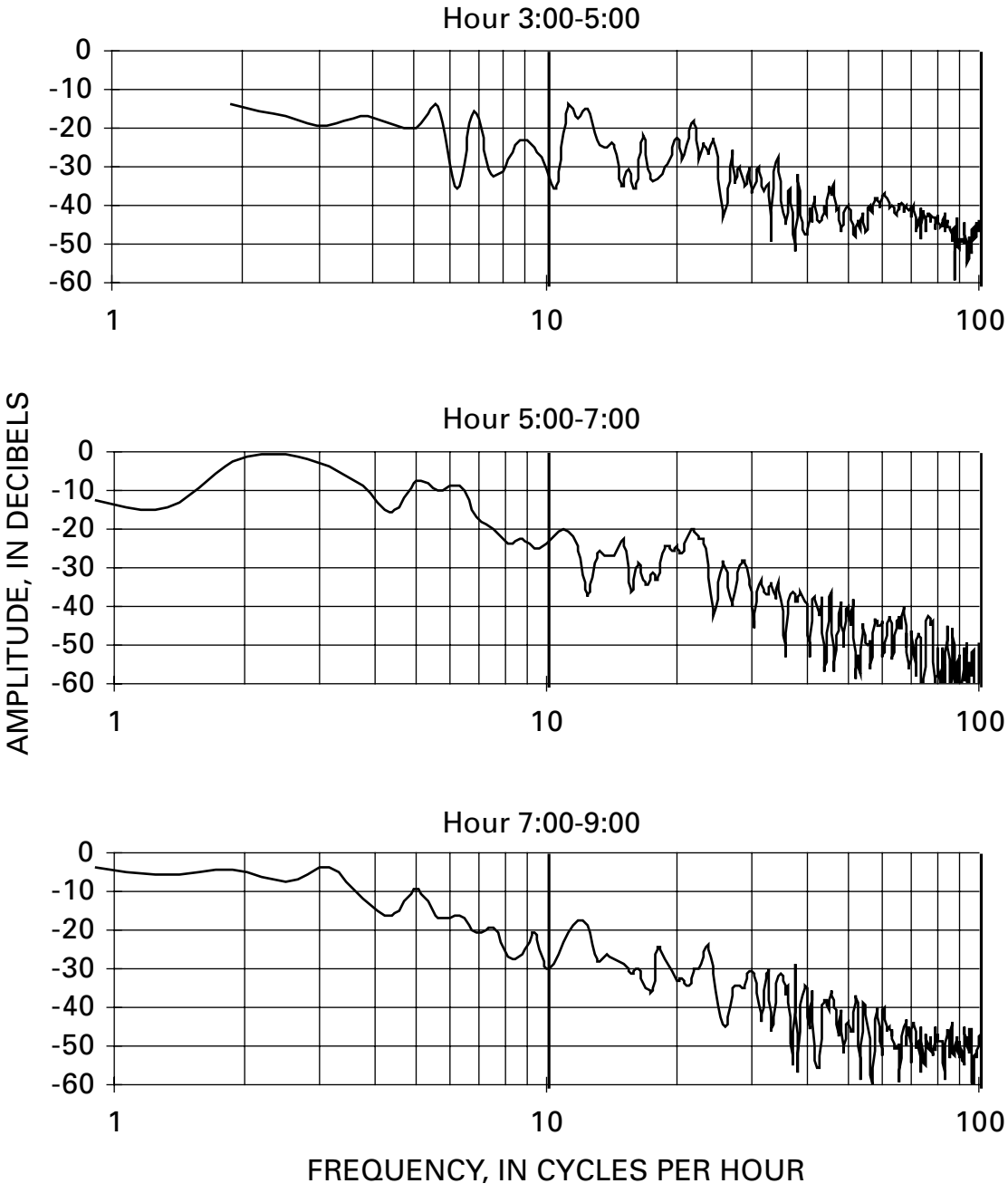

Figure 3.—Spectral analysis of 1906 tide-gauge record for three 2-hour time windows: immediately before (top), during (middle), and after (bottom) passage of initial tsunami. Spectral analysis was performed on residual (tidal component removed) record, using a 1,024-point fast Fourier transform.

calculated from elastic-dislocation theory (Okada, 1992), using different source parameters for the 1906 San Francisco earthquake, as described in the next section. The water-depth-dependent bottom-friction coefficients are the same as those described by Cheng and others (1993). Baroclinic forcing is not considered in this application of the TRIM model, and so initial conditions for salinity do not need to be specified. Similarly, a turbulent-closure scheme used in the model of Cheng and others is not used in this study, although Sato (1996) incorporated a similar scheme to model the effects of wave breaking for much larger tsunamis. One particular advantage of the TRIM model is that the emergence and flooding of shallow and low-lying areas are properly accounted for (Cheng and others, 1993).

Because the source region for the tsunami is along the Golden Gate platform (fig. 1), offshore bathymetry was appended to the bathymetric-data base for San Francisco Bay in the study by Cheng and others (1993). The bathymetry for San Francisco Bay was merged with a gridded offshore bathymetric-data base digitized from hand-contoured maps of U.S. Geological Survey soundings from several cruises in the region. The grid spacing used to model the tsunami from the 1906 San Francisco earthquake was 250 m, corresponding to the gridded bathymetry available for San Francisco Bay most recently used by McDonald and Cheng (1997). A 35-s time interval was used to model the evolution of the tsunami, which is much less than the 9-minute time interval used to model tidal circulation. Because the TRIM model uses the semi-implicit numerical scheme described above, the time interval is not required to satisfy the CFL stability condition (Δt 5.6 s) that applies to fully explicit finite-difference methods.

To estimate how much the results depend on the particular hydrodynamic model used, we compare the synthetic marigram calculated by Ma and others (1991) with that calculated by using the TRIM model (fig. 4*A*). We use the offshore vertical displacement determined by Ma and others (1991) as initial conditions for the TRIM model. Although the published figure showing the marigram comparison is very small (Ma and others, 1991, fig. 1b), we seem to have approximately reproduced the results of Ma and others (1991) by using the TRIM model. The only difference is that the oscillations after the initial negative pulse may be slightly larger with the TRIM model than with the linear long-wave model of Ma and others.

Offshore-Rupture Scenarios

We compared modeled tsunami time series at the Presidio tide-gauge station generated by different offshore-rupture scenarios with the observed record. Rather than constructing an inverse model to determine the source parameters for the tsunami, as did Ma and others (1991), we constructed forward models of the tsunami from geodetic analysis (Thatcher and others 1997), geophysical imaging, and coastal ground-failure observations soon after the earthquake (Lawson, 1908). The first and most likely set of offshore-rupture scenarios are those in which the tsunami is generated solely by slip along either continuous or discontinuous strands of the San Andreas Fault, as interpreted by Jachens and Zoback (1999) and Zoback and others (1999). The second set of offshore rupture scenarios involve slip on nearby faults in addition to the San Andreas Fault. In addition to tsunamis generated by coseismic deformation, we consider a third set of scenarios in which the tsunami is generated by local cliff failures. The predicted and observed tsunami marigrams for each scenario are compared in figures 4 through 7.

For the first set of offshore-rupture scenarios, we use coseismic slip values for the 1906 earthquake rupture interpolated in the offshore region between the Tomales Bay and Colma local geodetic networks by Thatcher and others (1997). Our first objective is to determine whether we can use the tide-gauge record to discriminate between continuous and discontinuous rupture on offshore strands of the San Andreas Fault in generating the tsunami. First, we calculate the tsunami derived from rupture on a continuous strand of the San Andreas Fault. The fault trace is identical to that used by Thatcher and others (1997) in their geodetic analysis. The dominant source region (that is, the region with the largest static vertical displacement) extends over a broad area near the fault bend, directly across from the Golden Gate (fig. 1). Thus, the amplitude of the first arrival from the computed tsunami is smaller and arrives earlier than what was observed (fig. 4*B*).

We also tested three discontinuous-rupture scenarios to explain the observed tsunamis, using surface traces of the San Andreas Fault as interpreted by Jachens and Zoback (1999) and Zoback and others (1999). Because the available seismograms for the 1906 San Francisco earthquake do not permit a detailed analysis of local changes in source parameters, we use a genetically similar event as a proxy for the 1906 rupture. The fault geometry for the 1906 earthquake is patterned after the source geometry of the 1995 Kobe, Japan, $M_w = 6.9$ earthquake from the detailed analysis by Wald (1996) and Spudich and others (1998). In the 3-km right-stepover region offshore of Lake Merced (fig. 1), the overlapping strands were specified as dipping 83º toward each other, such that the fault segments intersect at a presumed hypocentral depth of 10 km for the 1906 earthquake. This is one possible model of how rupture can be facilitated through a stepover region. However, because we cannot invert the tsunami or seismic-waveform data to determine the detailed fault geometry in the stepover region, the antithetic fault structure fashioned after the 1995 Kobe, Japan, earthquake may not uniquely explain the 1906 tsunami record. For this stepover fault geometry, the initial tsunami amplitude is considerably greater (fig. 4*C*) than for the tsunami modeled by using a continuous fault trace (fig. 4*B*). The resulting tsunami record more closely matches the predicted first-arrival time (fig. 4*C*) than does the synthetic record derived from continuous rupture on the San Andreas Fault (fig. 4*B*). Nonvertical fault dips in the stepover region result in a greater amount of subsidence, and so the predicted peak negative amplitude in figure 4*C* is larger than for the

synthetic record shown in figure 4*B*, though still less than the observed peak negative amplitude.

The second discontinuous-rupture scenario involves both the right stepover and a smaller 1-km left stepover near Bolinas Lagoon (fig. 4*D*). In comparison with the single-stepover scenario, inclusion of the second stepover results in only slight changes to the synthetic marigram: short-period fluctuations are observed before the peak negative deflection.

The third discontinuous-rupture scenario involves two stepovers as before, but with a local change of rake to –172º

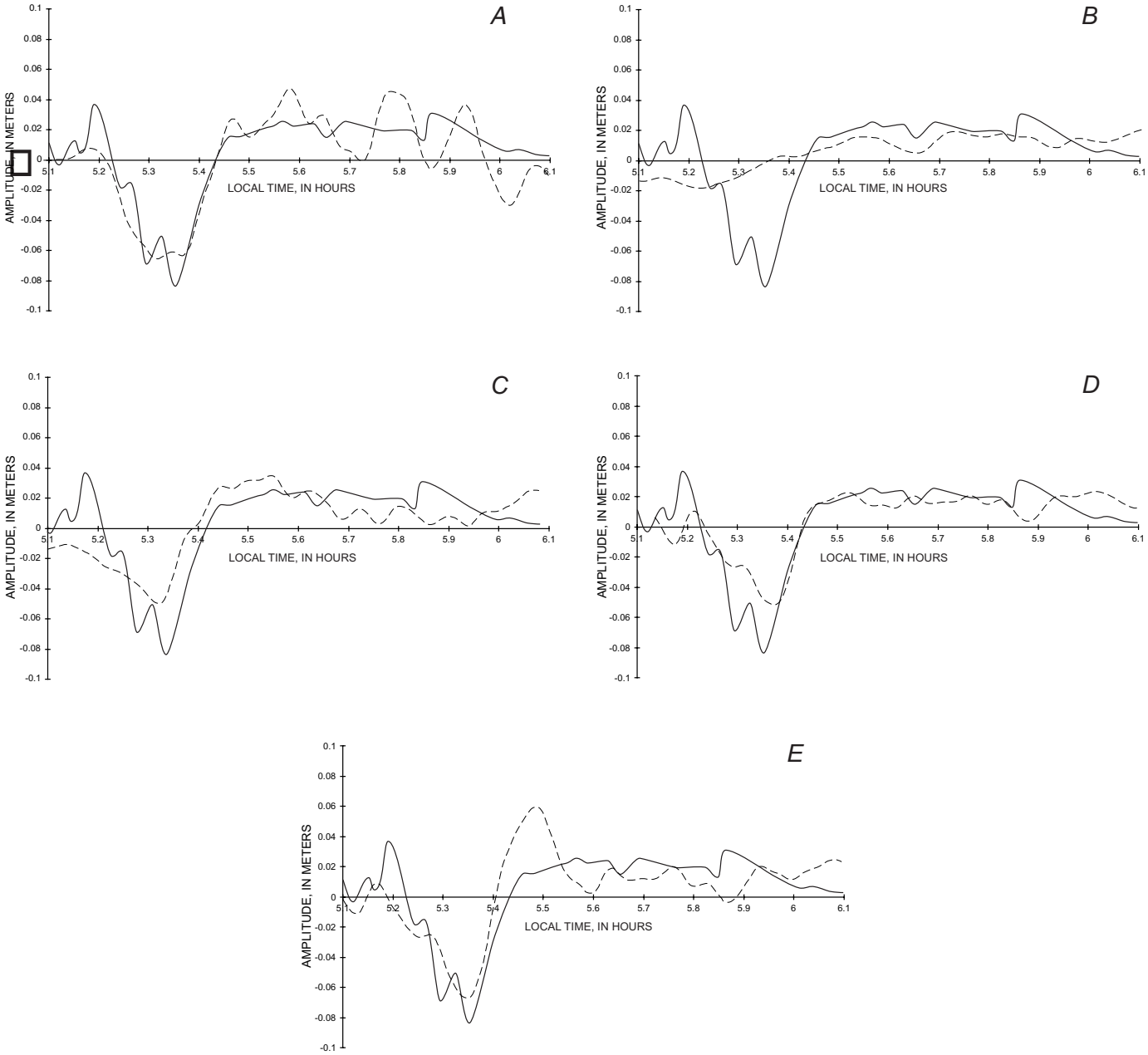

Figure 4.—Observed, residual marigram (solid curve) and synthetic marigram (dashed curve) at the Presidio tide-gauge station calculated for different initial conditions. *A*, Using sea-floor displacement values of Ma and others (1991) calculated from inversion of tide-gauge record (rather from forward modeling using elastic-dislocation solutions, as in this study), such that a good fit with observed marigram is expected. *B*, Using initial conditions specified by static, elastic displacements for rupture on a continuous trace of the offshore San Andreas Fault (fig. 1). *C*, Using initial conditions specified by static, elastic displacements for rupture on a discontinuous trace of the offshore San Andreas Fault that includes a single dilatational stepover north of Lake Merced (fig. 1). Note that observed record is shifted over time with respect to other scenarios by an amount that is within uncertainty of origin time. *D*, Using initial conditions specified by static, elastic displacements for rupture on a discontinuous trace of the offshore San Andreas Fault that includes both dilatational stepover north of Lake Merced and a smaller compressional stepover south of Bolinas Lagoon (fig. 1). *E*, Using initial conditions specified as in figure 4*D*, but with a local change of rake to 172° for fault segments bounding dilatational stepover.

in the region of the right stepover (fig. 4*E*). Like the assignment of dipping fault segments in the stepover region, the additional assignment of a local change in rake is modeled after the source parameters of the 1995 Kobe, Japan, earthquake. This change results in greater downdropping in the stepover region and thus a larger negative amplitude of the first arrival (fig. 4*E*). Although the ratio of the synthetic to observed peak negative amplitude is close to 1 for the this scenario, a trailing positive phase is evident on the synthetic marigram but not on the tide-gauge record. Although an optimal fit that accounts for both the peak negative amplitude of the first arrival and the absence of a trailing positive phase cannot be made with the three discontinuous-rupture scenarios considered, the timing and amplitude predicted from these scenarios strongly support the inference that the 1906 earthquake rupture occurred on discontinuous strands of the offshore San Andreas Fault.

The tsunami is affected not only by the source parameters of the earthquake but also by the response of the surrounding material. The foregoing analysis assumed that the blocks adjacent to the fault deformed as a Poisson solid ($\nu = 0.25$). Natural variations in the Poisson ratio due to rock type only slightly affect the resulting tsunami (Geist, 1998). For such large events as the 1906 San Francisco earthquake, however, the bulk strength of much of the surrounding material may have been exceeded, such that the effective Poisson ratio was greatly increased. This result is somewhat inconsistent, however, with patterns of permanent deformation that indicate localized subsidence within the graben defined by the dilatational stepover (see next section). To determine the effect on the tsunami from a material that closely preserves volume during deformation, we recalculate the scenarios in figures 4*B*, 4*C*, and 4*E*, using a Poisson ratio near 1/2 ($\nu = 0.45$) (fig. 5). Changes in the synthetic marigrams for the continuous-rupture scenario (fig. 4*B*) are subtle. However, using a high Poisson ratio for the discontinuous-rupture scenario without a local change in rake (fig. 4*C*) results in a larger peak negative amplitude, closer to what was observed. The conclusion that the tsunami resulted from discontinuous rupture remains unchanged, although it remains unclear whether the 10-cm deflection recorded at the Presidio tide-gauge station was caused by a local change in rake in the stepover region or by postelastic failure during the earthquake in the offshore region.

Other scenarios for the source of the tsunami from the 1906 San Francisco earthquake can also be envisioned. For example, localized coseismic slip on neighboring faults may have occurred. Combined slip on the San Gregorio and San Andreas Faults results in slight changes to the coda of the tsunami but does not greatly alter the signature of the first arrival. In addition, normal faulting on the Golden Gate platform (fig. 1) is indicated by seismic-reflection data and focal mechanisms (Zoback and others, 1999). Combined slip on a continuous strand of the San Andreas Fault and on a normal fault west of the San Gregorio Fault does not significantly increase the amplitude of the tsunami at the Golden Gate over using a continuous rupture on the San Andreas Fault alone (fig. 6), primarily because earthquake-scaling relations permit only a limited amount of slip for the maximum possible length of normal faults in the offshore region.

Finally, ground shaking from the earthquake may have caused a massive seacliff failure as the source for the tsunami. One particular example of seacliff failure was well documented by Lawson (1908). Near Mussel Rock, where the onshore strand of the San Andreas Fault south of the stepover intersects the coastline, Lawson noted that "The cliff was severely shaken, and great quantities of earth and rock were caused to fall or slip down." Although it is exceedingly difficult to formulate an accurate model of a tsunami generated from slides without knowing the exact dimensions and time history, traveltime information for the tsunami alone can be used to test whether seacliff failures may have caused or contributed to the tsunami. For the Mussel Rock landslide, the tsunami would have arrived too late to explain the record at the Presidio tide gauge station (fig. 7). Likewise, a possible slide near Point Bonita would have arrived too early (fig. 7). In summary, in only a few places could a massive slide triggered by the earthquake have occurred to explain the observed arrival time of the tsunami.

Discussion

Implications for Rupture Mechanics

The conclusion that the 1906 earthquake rupture occurred on discontinuous fault strands has specific implications for the rupture mechanics of this section of the San Andreas Fault. The influence of dilatational stepovers (for example, north of Lake Merced, fig. 1) and compressional stepovers (for example, south of Bolinas Lagoon) on the mechanics of fault rupture has been studied by using quasi-static models by Segall and Pollard (1980) and by using dynamic models by Harris and others (1991), Harris and Day (1993), and Kase and Kuge (1998). Results from these models indicate that generally rupture is facilitated at dilatational stepovers and inhibited by compressional stepovers. Whether dynamic rupture propagates through a stepover region, however, depends on the separation distance, the velocity of rupture, and the state of pore pressure (Harris and Day, 1993). Because of the small separation distance of the compressional stepover south of Bolinas Lagoon (fig. 1), the stepover would probably not present a barrier to rupture propagation. In addition, given the dimension of the dilatational stepover north of Lake Merced, a fault rupture propagating from either the north or the south would probably propagate through the stepover, unless the pore fluids in the region were in an "undrained" state (see Sibson, 1985, 1986). More information on the geometry and secondary faulting of the dilational stepover is needed to critically assess whether this stepover may be a likely barrier to rupture propagation.

The fact that the epicenters for both the 1906 San Francisco earthquake (as determined by Bolt, 1968, and Boore, 1977) and the 1995 Kobe, Japan, earthquake occurred at dilatational stepovers also suggests that the state of stress in these

regions facilitates not only continued propagation of rupture but also initiation of rupture (Zoback and others, 1999). Because the orientation of principal stresses varies with the geometry of the stepover region (Rodgers, 1980; Segall and Pollard, 1980), probably only those stepovers with a specific range of fault overlap can serve as sites for preferential earthquake initiation. Although some progress has been made in determining whether stepovers serve as barriers to rupture propagation, little theoretical work has examined the state of initial stress at stepover regions during the period when faults are locked.

Inferred Long-Term Rates of Subsidence

An approximately 3-km-wide Pliocene and Quaternary basin that may be an older equivalent of the active pullapart basin offshore is exposed onland directly northeast of the San Andreas Fault on the northernmost part of the San Francisco peninsula, in the sequence of ~3.0- to 0.2-Ma shallow marine to estuarine deposits known as the Pleistocene Merced Formation (Ingram, 1992). Jachens and Zoback (1999) interpreted detailed gravity data on the northern part of the peninsula to indicate a 2- to 3-km-wide, southeast-trending trough filled locally with more than 1 km of young deposits, bounded on the southwest by the onshore San Andreas Fault and on the northeast by the onshore extension of the right-step strand. This trough coincides closely with the narrow belt of outcropping Merced Formation and shallows gradually to the southeast over a distance of about 10 km, just as the Merced Formation thins to the southeast. Hengesh and Wakabayashi (1995) argued that the Merced Formation was deposited in a marine basin developed within a pullapart structure which has migrated with the Pacific Plate (and currently lies offshore from the Golden Gate, fig. 1), an interpretation consistent with the geophysical data.

The tsunami modeling presented here suggests that the estimated 3.65 to 4.5 m of strike-slip offset in the 1906 San Francisco earthquake on the Golden Gate platform (fig. 1; Thatcher and others, 1997) may have been accompanied by an average tectonic subsidence of about 0.65 m within a 6.25-km^2 area centered on the stepover. Assuming that the right stepover in the San Andreas Fault is a long-term geologic feature which represents a "moving" depocenter for the Merced Formation (Hengesh and Wakabayashi, 1995), then this "secondary" subsidence accompanying major strike-slip earthquakes can be compared with geologically determined subsidence rates for the Merced Formation. The estimated recurrence interval for large San Andreas Fault events ranges from 250 to 300 years (Schwartz and others, 1998). If the ratio of subsidence to horizontal slip that occurred here in 1906 is typical, this interval implies a subsidence rate of 2.36 m per 10^3 years (0.65 m per 275 yr), substantially greater than the geologically estimated subsidence rate of about 0.6 m per 10^3 years determined from a total of 1,750 m of sedimentary section accumulated over 2.9 m.y. Clifton (1988) originally suggested a subsidence rate of 1 to 1.5 m per 10^3 years for the Merced Formation, assuming that it was entirely Pleistocene (past 1.6 m.y.). Ingram (1992) used Sr-isotopic data and sedimentation rates to determine ages of 3.1 Ma for the base of the formation and about 0.2 Ma for the top—hence our updated rate. The source of the discrepancy may be that much of the slip on the San Andreas Fault occurs along shorter segments that do not break through the Golden Gate stepover. In addition, possible interevent changes in the rake of the slip vector, as well as the overall complexity of rupture through the stepover region, makes quantification of long-term subsidence rates difficult. More research is needed to reconcile the coseismic deformation inferred from the 1906 earthquake with long-term geologic observations along the Golden Gate platform.

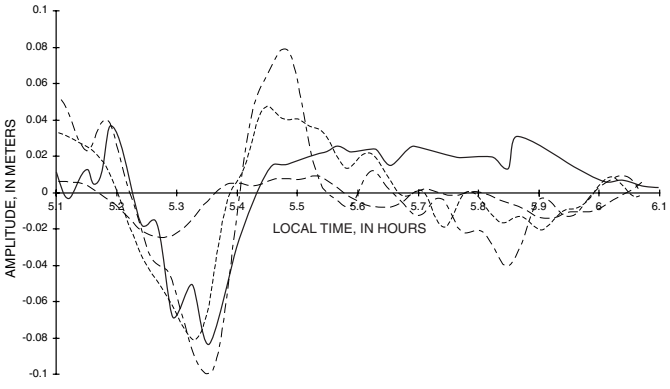

Figure 5.—Observed, residual marigram (solid curve) and synthetic marigrams calculated using a Poisson ratio (*n*) of 0.45 for initial conditions in figures 4*B* (long-dashed curve), 4*C* (short-dashed curve), and 4*E* (alternating short- and long-dashed curve).

Tsunami Hydrodynamics at the Entrance to San Francisco Bay

In comparison with tsunamis generated more commonly by subduction-zone earthquakes, the propagation of the tsunami generated by the 1906 San Francisco earthquake is highly unusual. Because the dominant source region for the tsunami (the 3-km right stepover) is very near shore, the negative-polarity first arrival recorded at the Presidio tide-gauge station propagated northward as a trapped wave (fig. 8). This tsunami contrasts with tsunamis from subduction-zone earthquakes in which the largest coseismic displacements are typically far offshore and the first-arrival broadside from the source region propagates as a direct wave. For those rupture scenarios of the 1906 earthquake that result in large displacements at the stepover, soon after the negative-polarity phase leaves the source region, a positive phase emanates from the source region, as suggested by H.F. Reid (in Lawson, 1908) and as shown in early theoretical work by Momoi (1964). Because of the large-amplitude changes, horizontal currents near the source region are significantly higher than anywhere

else during propagation. It is unclear why a strong trailing positive pulse is not predicted at the Presidio tide-gauge station for the scenario with two stepovers and horizontal rake (fig. 4*D*). Analysis of the evolution of the tsunami wavefield indicates that although trailing pulses of opposite polarities are generated by the two stepovers, the phase propagating southward from the compressional stepover is scattered at Point Bonita before reaching the Golden Gate (fig. 8), such that the positive trailing pulse from the dilatational stepover is not obviously eliminated through destructive interference. The combination of a complex shoreline geometry and a nearshore source that excites coastally trapped edge waves precludes a simplified analysis of observed phases at the Presidio tide-gauge station.

Although it is difficult to track individual phases of the tsunami, coastally trapped edge waves do seem have caused the fluctuations observed in the coda of the tsunami record, with an apparent period of 40 to 45 minutes. Edge waves propagate parallel to the shoreline and occur in distinct modes, with highest amplitudes near the shoreline (LeBlond and Mysak, 1978; Carrier, 1995). Sharp changes in the shape of the shoreline will cause edge waves to scatter, reflect back, and generate nontrapped modes. The phase and group velocity for edge waves depend on the shelf slope (Ishii and Abe, 1980) and are typically much lower than for nontrapped modes. (Most of the nontrapped energy from the 1906 tsunami was directed offshore.) Largely because of edge waves, the response from a tsunami at different places along a coastline can vary drastically, as evidenced by the tsunami from the 1992 Cape Mendocino, Calif., earthquake (González and others, 1995). The dominant 40- to 45-minute period observed on the tide-gauge record of the 1906 tsunami most likely reflects the natural resonance of edge waves within the Gulf of the Farallones. The suggestion by Lawson (1908) that the 40- to 45-minute periodic waves resulted from reverberation within San Francisco Bay does not conform with the results from hydrodynamic modeling. The Golden Gate (fig.

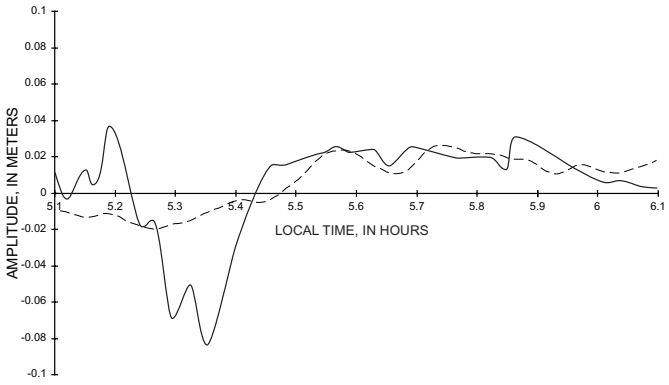

Figure 6. —Observed, residual marigram (solid curve) and synthetic marigram (dashed curve) at the Presidio tide-gauge station, calculated for initial conditions specified by static, elastic displacements for coseismic rupture on an offshore normal fault in addition to continuous rupture of the San Andreas Fault (fig. 4*B*).

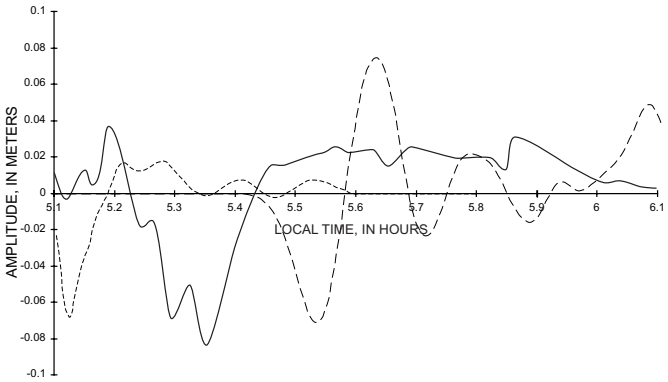

Figure 7.—Observed, residual marigram (solid curve) and synthetic marigram (dashed curve) at the Presidio tide-gauge station calculated for initial conditions specified by coseismically triggered seacliff failures at Mussel Rock (long-dashed curve) and at Point Bonita (short-dashed curve). Initial conditions are assumed such that predicted amplitude of marigrams is arbitrary. Traveltime predictions alone argue against generation of tsunami by seacliff failure.

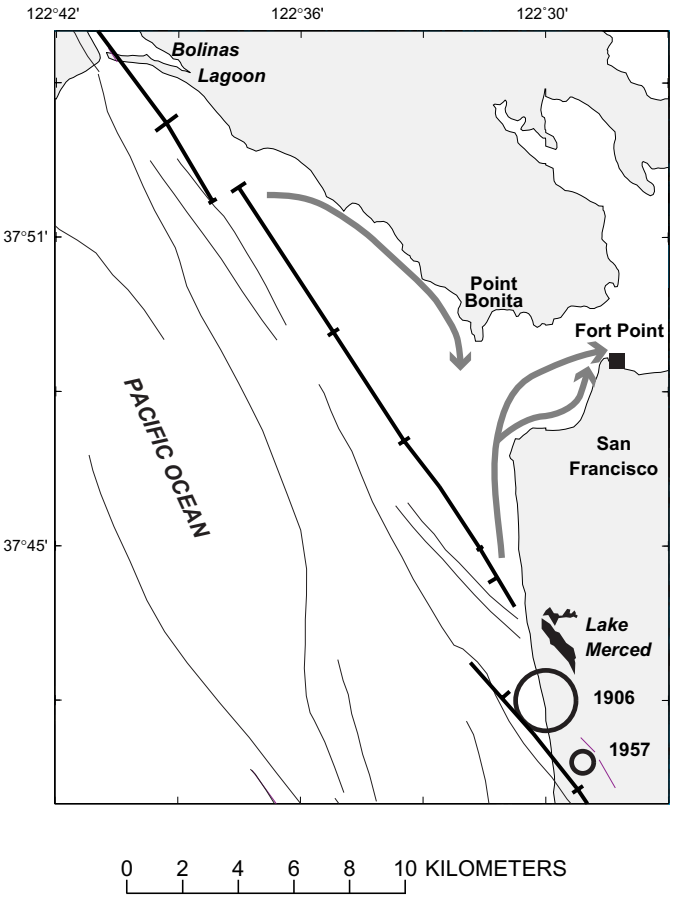

Figure 8.—San Francisco Bay region, showing primary pathways for tsunami first arrivals generated by dilatational stepover (negative polarity) north of Lake Merced and by compressional stepover (positive polarity) south of Bolinas Lagoon. Most energy propagates as coastally trapped edge waves. Southward-propagating edge wave from compressional stepover is scattered at Point Bonita. Same symbols as in figure 1.

1) permits only a limited amount of tsunami energy to enter San Francisco Bay. Once through the Golden Gate, tsunami energy is further attenuated during slow propagation through the shallow reaches of the bay. Because little tsunami energy is reflected back through the Golden Gate from the bay, the most likely source of the periodic oscillations is reflected and scattered edge waves outside the Golden Gate.

Summary

On the basis of new interpretations of the fault geometry west of the Golden Gate (fig. 1) by Jachens and Zoback (1999) and Zoback and others (1999), we have shown that the tsunami from the 1906 San Francisco earthquake originated from localized coseismic subsidence associated with a 3-km dilatational stepover just offshore of Lake Merced. On the basis of traveltime, amplitude, and phase characteristics of the tsunami record, the 1906 earthquake rupture most likely occurred on discontinuous strands of the San Andreas Fault bounding the dilatational stepover. Although derivation of the tsunami from rupture on an antithetic fault structure in the stepover region with a small amount of dip slip (analogous to the 1995 Kobe, Japan, earthquake rupture) provides the best match to the tsunami record, we cannot reliably determine the uniqueness of this model of rupture through the dilatational stepover from these data alone. However, the fact that both the 1906 San Francisco and 1995 Kobe, Japan, earthquakes initiated at a dilatational stepover and propagated bilaterally suggests that the initial state of stress at dilatational stepovers is conducive to the initiation of such large events. We have also shown in this study that estuarine-circulation models, such as that constructed for San Francisco Bay by Casulli (1990) and Cheng and others (1993), are particularly well suited to study near-shore, local tsunamis. The evolution of the tsunami wavefield predicted by this model indicates that (1) the first arrival at the Presidio tide-gauge station was primarily a coastally trapped edge wave, (2) tsunami wave energy was restricted through the Golden Gate such that reverberation within San Francisco Bay is unlikely the source of the 40- to 45-minute oscillations in the coda of the tsunami record, and (3) instead, the source of these oscillations is most likely the natural resonance of reflected and scattered edge waves within the Gulf of the Farallones.

Acknowledgments

We gratefully acknowledge reviews of the manuscript by Tom Parsons and Patrick Hart, editing by George Havach, and engaging discussions with Robert Simpson, Ralph Cheng, Jeff Gartner, and Kuo-Fong Ma.

References Cited

Bolt, B.A., 1968, The focus of the 1906 California earthquake: Seismological Society of America Bulletin, v. 58, no. 1, p. 457–471.

Boore, D.M., 1977, Strong-motion recordings of the California earthquake of April 18, 1906: Seismological Society of America Bulletin, v. 67, no. 3, p. 561–577.

Bortugno, E.J., McJunkin, R.D., and Wagner, D.L., 1992, Map showing recency of faulting, San Francisco-San Jose quadrangle, California: California Division of Mines and Geology Regional Geologic Map Series Map 51, sheet 5, scale 1:250,000.

Bowditch, Nathaniel, 1966, American practical navigator: Washington, D.C., U.S. Navy, Hydrographic Office, 1,524 p.

Bürgmann, Ronald, Arrowsmith, J.R., Dumitru, Trevor, and McLaughlin, R.J., 1994, Rise and fall of the southern Santa Cruz Mountains, California, from fission tracks, geomorphology, and geodesy: Journal of Geophysical Research, v. 99, no. B10, p. 20181–20202.

Carrier, G.F., 1995, On-shelf tsunami generation and coastal propagation, in Tsuchiya, Yoshito, and Shuto, Nobuo, eds., Tsunami; progress in prediction, disaster prevention and warning (Advances in Natural and Technological Hazards Research, v. 1): Dordrecht, Kluwer Academic Publishers, p. 1–20.

Casulli, Vincenzo, 1990, Semi-implicit finite difference methods for the two-dimensional shallow water equations: Journal of Computational Physics, v. 86, p. 56–74.

Cheng, R.T., Casulli, Vincenzo, and Gartner, J.W., 1993, Tidal, residual, intertidal mudflat (TRIM) model and its applications to San Francisco Bay, California: Estuarine, Coastal and Shelf Science, v. 36, no. 3, p. 235–280.

Clifton, H.E., 1988, Sedimentologic approaches to paleobathymetry with applications to the Merced Formation of central California: Palaios, v. 3, no. 5, p. 507–522.

Cooper, A.K., 1973, Structure of the continental shelf west of San Francisco, California: U.S. Geological Survey Open-File Report 73–1907, 65 p.

Cross, R.H., 1968, Tide gage frequency response: American Society of Civil Engineers Proceedings, Waterways and Harbors Division Journal, v. 94, no. 3, p. 317–330.

Das, Shamita, and Aki, Keitti, 1977, Fault plane with barriers; a versatile earthquake mode: Journal of Geophysical Research, v. 82, no. 36, p. 5658–5670.

Disney, L.P., and Overshiner, W.H., 1925, Tides and currents in San Francisco Bay: U.S. Coast and Geodetic Survey Special Publication 115, 125 p.

Eva, Claudio, and Rabinovich, A.B., 1997, The February 23, 1887, tsunami recorded on the Ligurian coast, western Mediterranean: Geophysical Research Letters, v. 24, no. 17, p. 2211–2214.

Foreman, M.G.G., 1993, Manual for tidal height analysis and prediction (revised): Sidney, British Columbia, Canada, Institute of Ocean Sciences Pacific Marine Science Report 77–10, 66 p.

Geist, E.L., 1998, Local tsunamis and earthquake source parameters, in Dmowska, Renata, and Saltzman, Barry, eds., Tsunamigenic earthquakes and their consequences (Advances in Geophysics, v. 39): New York, Academic Press, p. 117–209.

Geist, E.L., and Zoback, M.L., 1999, Analysis of the tsunami generated by the M_w 7.8 1906 San Francisco earthquake: Geology, v. 27, no. 1, p. 15–18.

González, F.I., Satake, Kenji, Boss, E.F., and Mofjeld, H.O., 1995, Edge waves and non-trapped modes of the 25 April 1992 Cape Mendocino tsunami: Pure and Applied Geophysics, v. 144, no. 3, p. 409–426.

Greenberg, D.A., Murty, T.S., and Ruffman, Alan, 1993, A numerical model for the Halifax Harbor tsunami due to the 1917 explosion: Marine Geodesy, v. 16, no. 2, p. 153–167.

Harris, R.A., and Day, S.M., 1993, Dynamics of fault interaction; paral-

lel strike-slip faults: Journal of Geophysical Research, v. 98, no. B3, p. 4461–4472.
Harris, R.A., Archuleta, R.J., and Day, S.M., 1991, Fault steps and the dynamic rupture process; 2-D numerical simulations of a spontaneously propagating shear fracture: Geophysical Research Letters, v. 18, no. 5, p. 893–896.
Hengesh, J.V., and Wakabayashi, John, 1995 Dextral translation and progressive emergence of the Pleistocene Merced Basin and implications for timing of initiation of the San Francisco peninsula segment of the San Andreas Fault, in Sangines, E.M., Andersen, D.W., and Buising, A.V., eds., Recent geologic studies in the San Francisco Bay area:, Society of Economic Paleontologists and Mineralogists, Pacific Section Special Publication 76, p. 47–54.
Holbrook, W.S., Brocher, T.M., ten Brink, U.S., and Hole, J.A., 1996, Crustal structure of a transform plate boundary; San Francisco Bay and the Central California continental margin: Journal of Geophysical Research, v. 101, no. B10, p. 22311–22334.
Ingram, B.L., 1992, Paleoclimatic and paleoceanographic studies of estuarine and marine sediments using strontium isotopes: Stanford, Calif., Stanford University, Ph.D. thesis, 236 pp.
Ishii, Hiroshi, and Abe, Kuniaki, 1980, Propagation of tsunami on a linear slope between two flat regions. pt. 1, Edge wave: Journal of Physics of the Earth, v. 28, no. 5, p. 531–541.
Jachens, R.C., and Zoback, M.L., 1999, The San Andreas Fault in the San Francisco Bay region, California; structure and kinematics of a young plate boundary: International Geology Review, v. 41, no. 3, p. 191–205.
Kase, Yuto, and Kuge, Keiko, 1998, Numerical simulation of spontaneous rupture processes on two non-coplanar faults; the effect of geometry on fault interaction: Geophysical Journal International, v. 135, no. 3, p. 911–922.
Lander, J.F., Lockridge, P.A., and Kozuch, M.J., 1993, Tsunamis affecting the west coast of the United States 1806–1992: Boulder, Colo., U.S. National Geophysical Data Center, NGDC Key to Geophysical Records Documentation 29, 242 p.
Lawson, A.C., chairman, 1908, The California earthquake of April 18, 1906; report of the State Earthquake Investigation Commission: Carnegie Institution of Washington Publication 87, 2 v.
LeBlond, P.H., and Mysak, L.A., 1978, Waves in the ocean (Oceanography Series, v. 20): Amsterdam, Elsevier, 602 p.
Loomis, H.G., 1983, The nonlinear response of a tide gage to a tsunami: Tsunami Symposium, Hamburg, Germany, 1983 Proceedings, p. 177–185.
Ma, K.F., Satake, Kenji, and Kanamori, Hiroo, 1991, The origin of the tsunami excited by the 1906 San Francisco earthquake: Seismological Society of America Bulletin, v. 81, no. 4, p. 1396–1397.
Marsden, Richard, Zoback, M.L., Dreger, D.S., Julian, B.R., Olson, J.A., and Parsons, T.E., 1995, M5.3 normal? faulting event adjacent to the San Andreas Fault on the San Francisco Peninsula [abs.]: Eos (American Geophysical Union Transactions), v. 76, no. 46, supp., p. 423–424.
McDonald, E.T., and Cheng, R.T., 1997, A numerical model of sediment transport applied to San Francisco Bay, California: Journal of Marine Environmental Engineering, v. 4, no. 1, p. 1–41.
Momoi, Takao, 1964, Tsunami in the vicinity of a wave origin (I): University of Tokyo, Earthquake Research Institute Bulletin, v. 42, no. 1, p. 133–146.
Myers, E.P., and Baptista, A.M., 1995, Finite element modeling of the July 12, 1993 Hokkaido Nansei-Oki tsunami: Pure and Applied Geophysics, v. 144, no. 3–4, p. 769–801.
Okada, Yoshimitsu, 1992, Internal deformation due to shear and tensile faults in a half-space: Seismological Society of America Bulletin, v. 82, no. 2, p. 1018–1040.
Peraire, J., Zienkiewicz, O.C., and Morgan, K., 1986, Shallow water problems; a general explicit formulation: International Journal for Numerical Methods in Engineering, v. 22, p. 547–574.
Poon, Y.K., Tang, Shih, and Wu, Jin, 1992, Interactions between rain and wind waves: Journal of Physical Oceanography, v. 22, no. 9, p. 976–987.
Rabinovich, A.B., 1997, Spectral analysis of tsunami waves; separation of source and topography effects: Journal of Geophysical Research, v. 102, no. C6, p. 12663–12676.
Reid, H.F., 1910, The mechanics of the earthquake, v. 2 of Lawson, A.C., chairman, The California earthquake of April 18, 1906; report of the State Earthquake Investigation Commission: Carnegie Institution of Washington Publication 87, 192 p. [reprinted, 1969].
Reid, R.O., and Bodine, B.R., 1968, Numerical model for storm surges in Galveston Bay: American Society of Civil Engineers Proceedings, Waterways and Harbors Division Journal, v. 94, no. 1, p. 33–57.
Rodgers, D.A., 1980, Analysis of pull-apart basin development produced by en echelon strike-slip faults, in Ballance, P.F., and Reading, H.G., eds., Sedimentation in oblique-slip mobile zones: International Association of Sedimentologists Special Publication 4, p. 27–41.
Satake, Kenji, Okada, Masami, and Abe, Kuniaki, 1988, Tide gauge response to tsunamis; measurements at 40 tide gauge stations in Japan: Journal of Marine Research, v. 46, no. 3, p. 557–571.
Sato, Shinji, 1996, Numerical simulation of the propagation of the 1993 southwest Hokkaido earthquake tsunami around Okushiri Island: Science of Tsunami Hazards, v. 14, no. 2, p. 119–134.
Schwartz, D.P., Pantosti, Daniela, Okumura, Koji, Powers, T.J., and Hamilton, J.C., 1998, Paleoseismic investigations in the Santa Cruz Mountains, California; implications for recurrence of large-magnitude earthquakes on the San Andreas Fault: Journal of Geophysical Research, v. 103, no. B8, p. 17985–18001.
Segall, Paul, and Pollard, D.D., 1980, Mechanics of discontinuous faults: Journal of Geophysical Research, v. 85, no. B8, p. 4337–4350.
Sibson, R.H., 1985, Stopping of earthquake ruptures at dilational fault jogs: Nature, v. 316, no. 6025, p. 248–251.
———1986, Rupture interactions with fault jogs, in Das, Shamita, Boatwright, John, and Scholz, C.H., eds., Earthquake source mechanics: American Geophysical Union Geophysical Monograph 37, p. 157–167.
Spudich, Paul, Guatteri, M.G., Otsuki, Kenshiro, and Minagawa, Jun, 1998, Use of fault striations and dislocation models to infer tectonic shear stress during the 1995 Hyogo-ken Nanbu (Kobe) earthquake: Seismological Society of America Bulletin, v. 88, no. 2, p. 413–427.
Thatcher, W.R., Marshall, G.A., and Lisowski, Michael, 1997, Resolution of fault slip along the 470-km-long rupture of the great 1906 San Francisco earthquake and its implications: Journal of Geophysical Research, v. 102, no. B3, p. 5353–5367.
Tinti, Stefano, and Piatanesi, Alessio, 1996, Numerical simulations of the tsunami induced by the 1627 earthquake affecting Gargano, southern Italy: Journal of Geodynamics v. 21, no. 2, p. 141–160.
Tsimplis, M.N., 1992, The effect of rain in calming the sea: Journal of Physical Oceanography, v. 22, no. 4, p. 404–412.

Wald, D.J., 1996, Slip history of the 1995 Kobe, Japan, earthquake determined from strong-motion, teleseismic, and geodetic data: Journal of Physics of the Earth, v. 44, no. 5, p. 489–503.

Wald, D.J., Kanamori, Hiroo, Helmberger, D.V., and Heaton, T.H., 1993, Source study of the 1906 San Francisco earthquake: Seismological Society of America Bulletin, v. 83, no. 4, p. 981–1019.

Zoback, M.L., Jachens, R.C., and Olson, J.A., 1999, Abrupt along-strike change in tectonic style; San Andreas Fault zone, San Francisco Peninsula: Journal of Geophysical Research, v. 104, no. B5, p. 10719–10742.